European Radiology (2019) 29:2436–2447
https://doi.org/10.1007/s00330-018-5784-5

HEPATOBILIARY-PANCREAS

New MRI features improve subtype classification of hepatocellular adenoma

Sylvain Bise[1] · Nora Frulio[1] · Arnaud Hocquelet[1] · Nicolas Alberti[1] · Jean-Frederic Blanc[2] · Christophe Laurent[3] · Hervé Laumonier[1] · Charles Balabaud[4] · Paulette Bioulac-Sage[4,5] · Hervé Trillaud[1,6]

Received: 18 July 2018 / Revised: 31 August 2018 / Accepted: 20 September 2018 / Published online: 6 December 2018

Abstract

Objective MRI is crucial for the classification of hepatocellular adenomas (HCA) into subtypes. Our objective was to review and increase MRI criteria for subtype classification and define the limits.

Methods Pathological and radiological data of 116 HCAs were retrospectively analyzed to investigate MRI features of HCA pathological subtypes. Risk for complication was also evaluated with regard to subtype and tumor size.

Results 38/43 (88%) HNF1α-mutated HCAs (H-HCAs) were discriminated by (*i*) *fatty component* (homogeneous or heterogeneous) and (*ii*) *hypovascular pattern*, with a sensitivity of 88% and a specificity of 97%. 51/58 (88%) inflammatory HCAs (IHCAs) displayed features of sinusoidal dilatation (SD) including three different patterns (global SD, atoll sign, and a new "crescent sign" corresponding to a partial peripheral rim, hyperintense on T2W and/or arterial phase with persistent delayed enhancement). Sensitivity was 88% and specificity 100%. However, some HCA remained unclassifiable by MRI: HCA remodeled by necrotic/hemorrhagic changes covering > 50% of the lesion, H-HCAs without steatosis, IHCAs without SD, β-catenin-mutated and unclassified HCAs. Regarding malignant transformation (5/116) and bleeding (24/116), none was observed when the HCA diameter was smaller than 5.2 cm and 4.2 cm, respectively.

Conclusion Based on the largest series evaluated until now, we identified several non-described MRI features and propose new highly sensitive and specific MRI criteria. With the addition of these new features, 88% of the two main HCA subtypes could be identified.

Key Points

- *HNF1α-mutated hepatocellular adenomas (H-HCA) are characterized by the presence of fat and hypovascular pattern in MRI.*
- *Inflammatory hepatocellular adenomas (I-HCA) are characterized by different patterns translating sinusoidal dilatation including the newly described crescent sign.*
- *No MRI specific pattern was identified for β-catenin-mutated HCA (b-HCA).*

Keywords Liver neoplasms · Adenoma, liver cell · Magnetic resonance imaging · Catenins · Retrospective studies

Sylvain Bise and Nora Frulio contributed equally to this work.

Electronic supplementary material The online version of this article (https://doi.org/10.1007/s00330-018-5784-5) contains supplementary material, which is available to authorized users.

✉ Nora Frulio
nora.frulio@chu-bordeaux.fr

[1] CHU de Bordeaux, Service d'imagerie diagnostique et interventionnelle, Hôpital Haut-Lévêque, F-33604 Pessac, France

[2] CHU de Bordeaux, Service d'hépato-gastroentérologie et oncologie digestive, Hôpital Haut-Lévêque, F-33604 Pessac, France

[3] CHU de Bordeaux, Service de Chirurgie hépato-biliaire et transplantation hépatique, Hôpital Haut-Lévêque, F-33604 Pessac, France

[4] Université de Bordeaux, INSERM, UMR 1053, F-33076 Bordeaux, France

[5] CHU de Bordeaux, Service de Pathologie, Hopital Pellegrin, F-33076 Bordeaux, France

[6] EA IMOTION (Imagerie moléculaire et thérapies innovantes en oncologie), Université de Bordeaux, F-33076 Bordeaux, France

Abbreviations

Ass1	Argininosuccinate synthase 1
AUROC	Area under the receiver operating characteristic
b-HCA	β-catenin-mutated HCA
b-IHCA	β-catenin-mutated inflammatory HCA
CRP	C-reactive protein
FNH	Focal nodular hyperplasia
H-HCA	HNF1α-mutated HCAs
HBP	Hepatobiliary phase
HCA	Hepatocellular adenoma
HCC	Hepatocellular carcinoma
IHCA	Inflammatory HCA
LFABP	Liver fatty acid-binding protein
MRI	Magnetic resonance imaging
SD	Sinusoidal dilatation
T2W	T2-weighted sequence
UHCA	Unclassified HCA

Introduction

Hepatocellular adenoma (HCA) is a rare benign liver tumor occurring mainly in middle-aged women using oral contraceptives [1, 2]. Pathologic classification of HCA [3, 4] distinguishes three main subtypes based on molecular analysis: (a) HNF1α-mutated HCAs (H-HCA) that are characterized by a fatty phenotype and negative liver fatty acid-binding protein expression (LFABP); (b) inflammatory HCAs (IHCA) that exit inflammatory pathological hallmarks [4–6] related to *JAK-STAT* pathway activation [7–9] and can also be *β*-catenin-mutated (b-IHCAs, 10% of IHCA); (c) β-catenin-mutated HCAs (b-HCA) that have a higher risk of malignant transformation [10–13].

Less than 10% of tumors remain unclassified (UHCA) [10]. Recently, among UHCA, a new subgroup has been described, named sonic hedgehog HCA (shHCA), characterized by the activation of the sonic hedgehog pathway [14]. Henriet et al also showed that argininosuccinate synthase 1 (ASS1) immunohistochemistry identified all the UHCA [15].

MRI is crucial to diagnose HCA. Until now, MRI features have been described on the basis of small cohorts (less than 50 patients) and identified only the typical appearance of the two major subtypes [16–19]: H-HCAs with severe and homogeneous steatosis, and IHCAs with marked sinusoidal dilatation. Indeed, MRI features remain unclear for the dominant subtypes (H-HCAs, IHCAs) that lack typical hallmarks and for other subtypes (b-HCAs and UHCAs).

The aim of this study was to review and increase MRI features in order to better identify the two major HCA subtypes and to define the limits in a large series of 116 HCAs using a pathologic-MRI correlation.

Patients and methods

Study design and patients

From January 2004 to April 2015, all consecutive patients with at least one confirmed HCA on liver specimen were identified within our pathological database from our institution and from affiliated hospitals (Supplementary Table 1). Patients with exploitable liver MRI with at least five sequences (see Supplementary Table 2) were included. Patients without adequate MRI data (no MRI or not all required sequences) were excluded. Thus, clinical, radiological, and pathologic data were collected and reviewed. Study was conducted in accordance with local regulations and data protection agency recommendations and patient consent was waived.

Histological analysis

To classify HCAs, the analysis was performed for all tissue specimens (Supplementary Table 2) by two experienced readers, blinded to clinical and radiological data.

MRI techniques

All MRI examinations were performed with a 1.5 T machine, and the same MRI protocol was performed for 41 patients from our institution and 45 patients from collaborating hospitals (Supplementary Table 2).

Image analysis

All MRI data were assessed retrospectively and independently by three abdominal radiologists, all blinded to pathologic, clinical, and biological data. The new MRI criteria (see section below) were also defined before radiologic review, and consensus was obtained for all criteria.

Classical MRI features

Underlying liver was evaluated (fat fraction, iron overload, cirrhosis, or other diffuse liver disease).

All previously described MRI features [16–18] were collected for each tumor. We focused our analysis on the two main classical features already described [16, 18]:

(1) Evaluation of tumor fat: distribution (homogeneous, strong and diffuse [16], or heterogeneous) and visual semi-quantitative assessment (steatosis intensity and spread within the lesion: absence = 0, low ≤ 30%, moderate = 30 to 60%, high ≥ 60%).
(2) Sign of sinusoidal dilatation considered very specific for IHCA: (*i*) lesion with marked hyperintensity on T2W and persistent delayed enhancement translating global

sinusoidal dilatation [16] or (*ii*) complete hyperintense peripheral rim on T2W, typically enhanced in the late vascular phase, with isointense and homogenous center similar to surrounding liver, known as the "atoll sign" [18].

New MRI features

In addition, two new features were considered:

(1) Hypovascular pattern: the tumor is hypointense on fat-suppressed T1-weighted images as compared to surrounding liver on plain images, mildly enhances at the arterial phase and is again hypointense on delayed phases after gadolinium administration, returning to the same signal as plain images, without any persistent enhancement (Fig. 1).
(2) Crescent sign: a peripheral portion of hyperintense rim on T2W and/or arterial phase with persistent delayed enhancement especially in tumors with steatotic or remodeled center (Fig. 2). This feature also represents sinusoidal dilatation.

In addition, the following three MRI features were analyzed: (a) necrotic/hemorrhagic changes reaching ≤ 50% or > 50% of the surface of the lesion on visual estimation, (b) myxoid changes (foci of markedly fluid-like hyperintensity on T2W with enhancement, different from cystic or necrotic area [20, 21], (c) hemosiderin deposits (characterized by in-phase signal dropout on chemical shift sequences [22]—and hyposignal on T2W).

Tumor classification: classic MRI criteria only versus classic and new MRI criteria

First, tumors were classified according to classical MRI criteria [16, 18] into: (*i*) H-HCA subgroup (lesion with strong, diffuse, and homogeneous signal dropout on out-phases sequence), (*ii*) IHCA subgroup (lesion with global sinusoidal dilatation and/or "atoll sign") and (*iii*) non-classifiable HCA (lesion without typical pattern).

Then, we used new MRI criteria to classify nodules into: (*1*) H-HCA subgroup: lesion with fatty component (homogeneous or heterogeneous) and hypovascular pattern, (*2*) IHCA subgroup: lesion with one of the three MRI features of sinusoidal dilatation including crescent sign, and (*3*) non-classifiable HCA: lesion without specific pattern.

Multiple HCAs and complications

Next, multiple HCA or adenomatosis cases were investigated (number of cases visible by imaging vs. pathological examination, HCA subtype involved).

Regarding complications, signs of malignant transformation (nodule-in-nodule appearance on T2W, and arterial phase and/or washout on delayed phase) and severity of bleeding [23] (intratumoral-grade I, intrahepatic-grade II, extrahepatic-grade III) were analyzed.

The association with other liver lesions was reviewed. Associated lesions were diagnosed by MRI whenever they were typical and by histology in the other cases.

Statistical analysis

Continuous variables were expressed as median (first–third quartile) and categorical variables as frequencies and percentages and compared using Wilcoxon rank-sum test, Kruskal–Wallis, chi-squared, or Fisher's exact tests, according to distribution of variables and number of cases. Diagnostic values of each tested parameter were measured by calculating area under the receiver operating characteristic (AUROC). These were compared as recommended by Delong et al [24] for all lesions whatever their size and after separating lesions > 5 cm, because HCA > 5 cm usually require surgery. The optimal cutoff was chosen according to Youden's Index. All reported *p* values were based on two-sided tests of significance. *P* value < 0.05 was considered as significant. Analyses were performed using STATA version 13.

Results

Demographics and general characteristics

Two hundred eighty-eight consecutive patients with at least one confirmed HCA on liver specimen were identified within our pathological database ($n = 143$ from our institution and $n = 145$ from affiliated hospitals). We included a cohort of 86 patients with exploitable liver MRI and suitable clinical pathology material. The other 202 cases were excluded due to lack of adequate MRI data.

Main clinical and pathological data are summarized in supplementary Table 1. Among the 86 patients included, 75 (87%) were female and median age was 40 (35–45) years. Thirty-six (42%) patients were overweight (BMI > 25 kg/m^2) and this feature was more commonly associated with IHCA subtypes than with H-HCA (54.5% vs. 23.5%, $p = 0.004$). History of oral contraceptive was documented in 60 (70%) patients (mean duration of use 16.8 years ± 8.3) and most nodules were incidentally discovered (35/86). Median tumor size was 5 (3–8) cm. Interestingly, b-HCA size was significantly greater than in other subgroups with a median size of 10 (9–11) cm vs. IHCA 5 (3–7) cm, H-HCA 4.9 (2–6) cm, and UHCA 8 (5.1–10) cm ($p = 0.018$). On MRI, 37/86 patients had

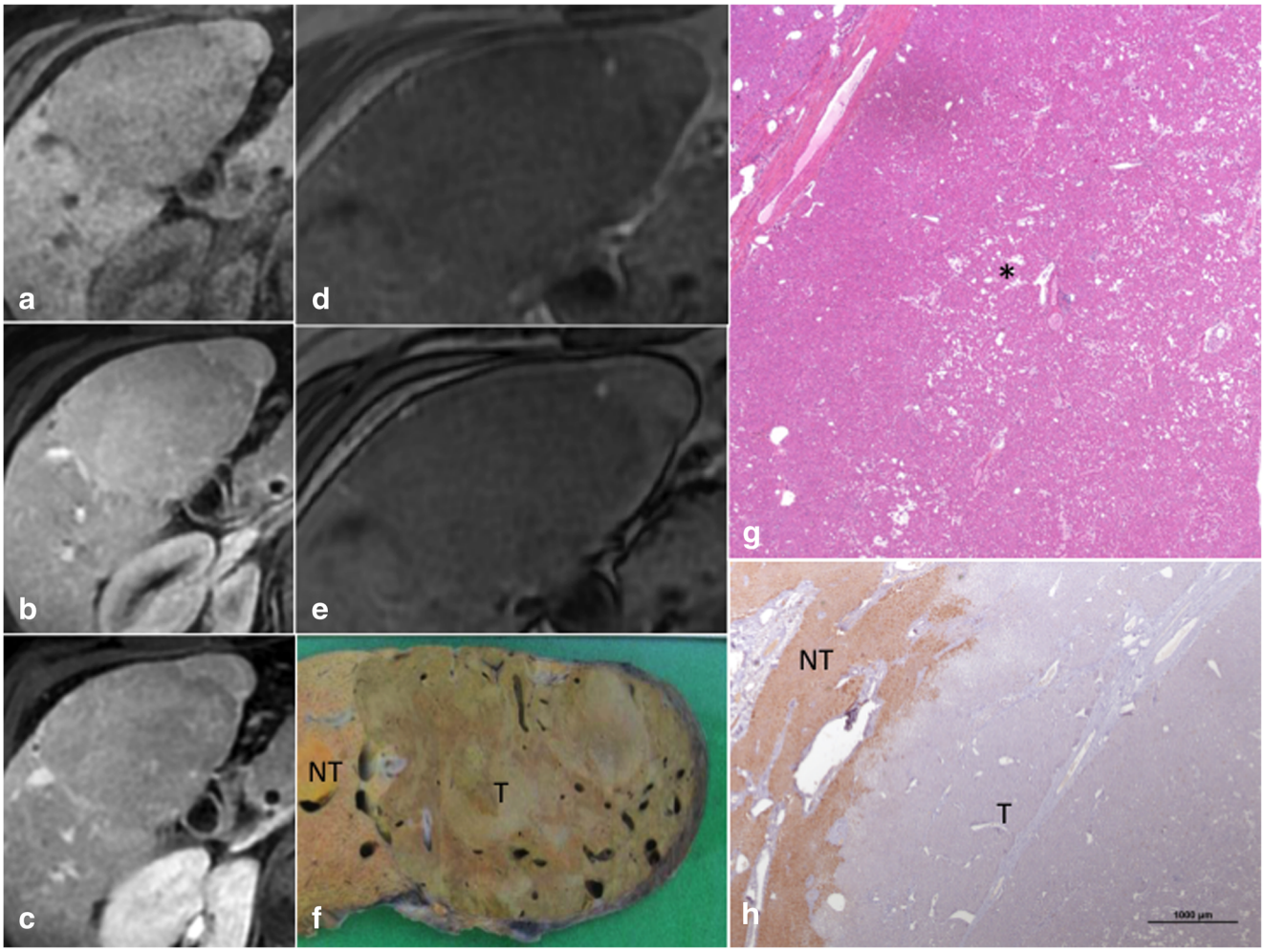

Fig. 1 Low steatotic HNF1a-inactivated hepatocellular adenoma (H-HCA) with hypovascular pattern. **a**, **b**, **c** Axial three-dimensional fat-suppressed gradient-echo T1-weighted acquisitions before (**a**) and after injection of gadolinium chelate at the arterial (**b**) and portal venous phase (**c**). *Hypovascular pattern*: lesion (85 mm; segment V) hypointense (**a**) with low arterial enhancement (**b**), and return to initial signal at portal phase, without any persistent enhancement (**c**); in (**a**) and (**c**), the tumor is hypointense compared to surrounding liver. **d**, **e** In phase (**d**) and opposed phase (**e**) T1-weighted image. The signal dropout on out-phase (**e**) is very weak; (**f**) *formalin-fixed surgical specimen*, irregularly colored tumor (T) from white to clear brown, clearly different from non-tumoral liver (NT); **g** *H&E*, tumor made of benign hepatocytes intermingled with thin vessels, no steatosis in this area but minimal myxoid changes (*); (**h**) *LFABP immunostaining*, no expression of LFABP in T contrasting with normal expression in NT

one nodule, 16 had 2–4, 12 had 5–9, and 21 patients had more than 10 nodules (adenomatosis).

Liver steatosis was identified in 27/86 (31%) patients and most of them displayed IHCAs (16/27, 59%). Iron overload in liver was found in 1 case (IHCA) and vascular liver disorder in 2 cases (1H-HCAs and 1b-IHCA). No liver dysmorphia or cirrhosis was identified.

Associated liver tumors were observed in 13 patients: 11 focal nodular hyperplasia (FNH—8/13 patients), 5 hemangiomas (3/13 patients), 1 angiomyolipoma, 1 concomitant hepatocellular carcinoma (HCC), and 1 biliary hamartomas. Three patients displayed 2 FNHs (one had 1 hemangioma in addition) and one patient 3 hemangiomas. FNHs were associated to IHCA, H-HCA, and b-HCA in 4, 2, and 2 out of 8 cases, respectively.

MRI features and HCA subtypes (Table 1 and 2)

H-HCA MRI features ($n = 43$)

Steatotic appearance was predominant. Fatty component was high in majority of cases (30/43, 70%). Only 10/43 (23%) H-HCAs were moderately fatty, 2/43 (5%) were low in fat, and one (2%) H-HCA had no fatty content. Twenty-nine (67.4%) H-HCAs displayed a typical strong and diffuse homogeneous signal dropout in opposed-phase gradient-echo sequence described as 100% specific by Laumonier et al [15]. All H-HCAs identified by Laumonier's criteria showed "hypovascular pattern." Moreover, among the 14 H-HCA from outside Laumonier's criteria with heterogeneous or no fatty component (Table 1), 9 presented a stereotyped

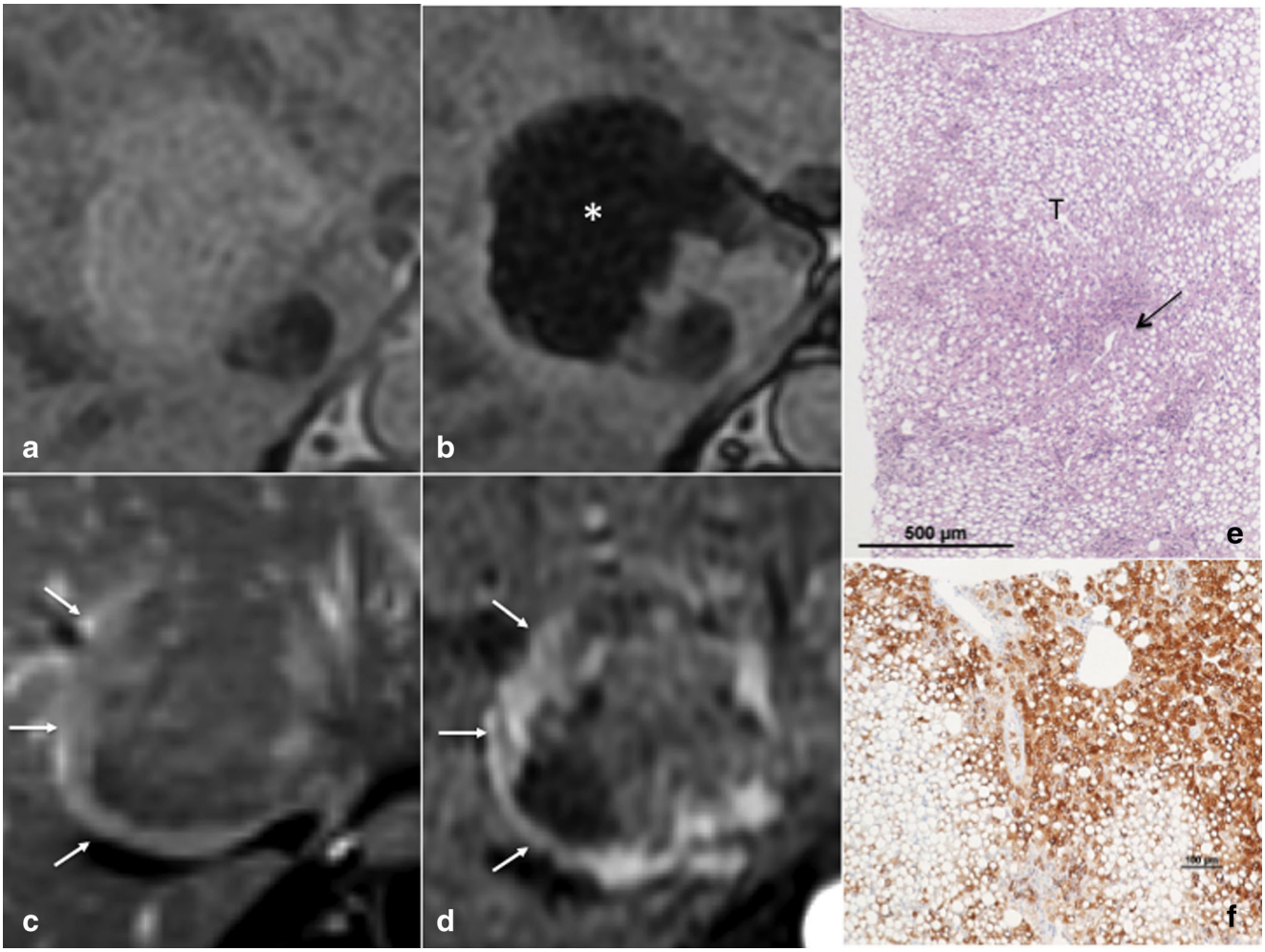

Fig. 2 Steatotic inflammatory HCA (IHCA) with "crescent sign" of sinusoidal dilatation on MRI. **a**, **b** In phase (**a**) and opposed phase (**b**) T1-weighted gradient-echo sequence. Highly steatotic tumor (5 cm; segment VIII) with strong signal dropout on out-phase **b** of central area (*); **c, d** Axial T2-weighted fat-suppressed (**c**) and three-dimensional fat-suppressed gradient-echo T1-weighted after injection of gadolinium chelate at the arterial phase (**d**). "*crescent sign*": hyperintense peripheral rim portion on T2W (**c**) with strong arterial enhancement (**d**) and persistent portal venous enhancement (not shown) after gadolinium administration; **e** biopsy of the tumor (T); *H&E*, benign steatotic hepatocytes, intermingled with inflammatory foci around thickened arteries (black arrow); **f** *CRP immunostaining*, all tumoral hepatocytes overexpressed CRP (less visible in reduced cytoplasm of steatotic hepatocytes). LFABP expression was normal (not shown)

"hypovascular pattern" (Fig. 1**).** Intratumoral areas of myxoid changes were observed in 2 H-HCA. This feature was not found in other subtype.

As shown in Table 2, the diagnostic performance increased significantly using the new criteria with an AUROC = 0.928 vs 0.837 for Laumonier's criteria alone ($p = 0.006$). Indeed, these new criteria allowed to correctly reclassify 9/14 (64%) H-HCAs. Finally, 5/43 (12%) H-HCAs remained non-classifiable using MR imaging.

Considering only the subgroup of small H-HCAs ≤ 5 cm without necrotic/hemorrhagic changes or with necrotic/hemorrhagic changes ≤ 50% of tumor area (n = 22/43), new criteria correctly classified 22/22 H-HCA with an AUROC = 1 vs 0.932 for Laumonier's criteria alone ($p = 0.069$).

IHCA MRI features (n = 58) (Tables 1 and 2)

A high proportion of IHCAs was characterized by isointensity (50%) or hyperintensity (21%) on T1-weighted sequences. Most of them (37/58) displayed classical global sinusoidal dilatation (n = 23) [15] or atoll sign (n = 14) [17] on MRI corresponding to an AUROC of 0.819. Fourteen (24%) IHCAs were steatotic in variable proportions: high for 2/58 cases, mild and low for 5/58 and 7/58, respectively. Among the 21/58 (36%) IHCAs unidentified by Laumonier's criteria, 14 (67%) presented the new peripheral crescent sinusoidal dilatation criterion (Fig. 2). Adding "crescent sign" to classical features significantly improved MRI accuracy with an AUROC of 0.939 ($p < 0.001$). In association with sinusoidal dilatation, central

Table 1 MRI-pathological correlation

HCA subtypes	Nb of HCAs	MRI—pathological data correlation
H-HCAs confirmed by pathological analysis	*43*	
Typical H-HCAs according to Laumonier et al[1]	*29 (67.4%)*	Entirely steatotic and LFABP- on pathological data
Atypical H-HCAs identified by new criteria[2]	*9 (21%)*	1 (11%) were high steatotic but heterogenous, 7 (78%) were mildly steatosic, 1 (11%) were low steatosic (Fig. 1)
H-HCAs non-classifiable by MR imaging	*5 (11.6%)*	1 H-HCA with myxoid changes (cystic-like T2w hyperintensity foci on MRI) and no steatotic component, was non-typeable both with MRI and microscopic findings but LFABP- on immunostaining
		4 tumors with necrotics/hemorrhagics changes (> 50% of the lesion) on pathological data presented atypical enhancement on MRI after gadolinium injection (strong arterial enhancement and/or persistent enhancement at delayed phases). One of them contained myxoid changes on pathological examination difficult to identify from edematous changes on MRI in a very remodeled tumor. One of them displayed foci of sinusoidal dilatation on pathological examination that corresponded to atypical enhancement but not to T2w hyperintensity on MRI.
I-HCAs (included b-IHCAs) confirmed by pathological analysis	*58*	
Typical I-HCAs according to Laumonier et al[3]	*37 (64%)*	23 (39%) with global sinusoidal dilatation, 14 (24%) with atoll sign
Atypical I-HCAs identified by new criteria[4]	*14 (24%)*	Crescent sign corresponded to sinusoidal dilatation area in outer part of the tumor on pathological examination. Central component of the tumors which led to MRI conventional criteria (3) misidentification was mainly: steatotic (7 cases, 50%—Fig. 2) necrotics/hemorrhagics (4 cases) or with hemosiderin deposits (Fig. 3) (3 cases—and fibrous 1 case).
Non-classifiable I-HCAs/b-IHCAs by MR imaging	*7 (12%)*	3 tumors with important necrotics/hemorrhagics changes (> 50% of the lesion) led to MRI analysis difficulty (sinusoidal dilatation vs. edema) were positively identified by microscopic and immunostaining findings (CRP+)
		4 tumors with no sinusoidal dilatation sign both on MRI and microscopic analysis were diagnosed by CRP+ immunostaining on pathological examination
		No MRI specific feature was found to discriminate b-IHCAs (14 lesions) from I-HCAs (44 lesions)
b-HCAs confirmed by pathological and molecular analysis	*6*	
Central scar or wash-out	*0*	
b-HCAs misclassified by MRI criteria	*2*	Two very steatotic tumors (high and mildly amount) displayed an hypovascular pattern on MR images and were LFABP+, CRP- but GS+/β-catenin+ on Immunostaining.
Non-classifiable b-HCAs by MR imaging	*4*	No specific MRI feature was found to identify these b-HCAs from other groups, especially from U-HCAs
U-HCAs confirmed by pathological analysis	*9*	
Non-classifiable U-HCAs	*9*	7 (77.7%) was necrotics and/or hemorrhagics (> 50% of the lesion) and led to both MRI and pathological analysis difficulties
		2 displayed no specific feature both on MRI and pathological analysis
Malignant transformation	*6*	
"Nod in nod" feature with strong arterial enhancement without delayed wash-out	*3*	1 H-HCA with 2 macroscopic foci of dysplasia in men with hepatic vascular disorders (Fig. 5); 1 b-IHCA with dysplastic area; 1 IHCA with borderline area in men with overweight;
"Nod in nod" feature with strong arterial enhancement and delayed wash-out	*1*	1 b-HCA with macroscopic area of HCC
Microscopic foci of malignant transformation non-identified by MRI	*2*	1 b-HCA with high heterogenous steatotic component and hypovascular pattern (Fig. 4); 1b-IHCA with severe necrotic changes

[1] Strong, homogenous, and diffuse signal dropout on chemical shift sequences

[2] Steatotic component (homogenous or heterogenous) with hypovascular pattern

[3] Global sinusoidal dilatation (T2w hyperintensity and persistent delayed enhancement) or atoll sign

[4] Croissant sign (croissant of sinusoidal dilatation outside of the tumor with a remodeled center)

Table 2 Comparison of diagnostic parameter test values (sensibility, specificity, negative predictive value, positive predictive value, AUROC) between classical Laumonier's MRI criteria and new MRI criteria

			Sensitivity (%)	Specificity (%)	Negative predictive value (%)	Predictive positive value (%)	AUROC (95% confidence interval)
H-HCA	All tumors	Old criteria	67.4	100	84	100	0.837 (0.766–0.908)
		New criteria	88.4	97.2	93	95	0.928 (0.876–0.980)
	Tumors < 5 cm	Old criteria	86.4	100	92	100	0.932 (0.831–0.982)
		New criteria	100	100	100	100	1 (0.936–1)
IHCA	All tumors	Old criteria	63.8	100	73.4	100	0.819 (0.756–0.881)
		New criteria	87.9	100	89.2	100	0.939 (0.897–0.981)
	Tumors < 5 cm	Old criteria	71.2	100	72.7	100	0.859 (0.740–0.938)
		New criteria	93.7	100	92.3	100	0.969 (0.884–0.997)

hemosiderin deposits were found in 13 (22%) IHCAs, a feature only found in this phenotype (Fig. 3). Finally, among the 7/58 (12%) non-classifiable IHCAs, using both standard and new criteria, 3/58 were largely remodeled by necrotic/hemorrhagic changes (> 50%) and the 4 others did not contain signs of sinusoidal dilatation, neither on MRI nor on microscopic examination (Table 1).

Considering only the subgroup of IHCAs ≤ 5 cm without remodeling or with remodeling ≤ 50% ($n = 32/58$), the new criteria correctly classified 30/32 IHCAs with an AUROC = 0.969 vs 0.859 for the classical criteria alone ($p = 0.003$). Among the 58 IHCAs, 14 (24%) were b-IHCAs; however, there was no pattern difference with non-β-catenin-mutated IHCAs on MRI.

b-HCA MRI features ($n = 6$)

No discriminant characteristics for lesion pattern were found for the 6 b-HCAs, specifically no significant scar or delayed washout after injection. Nonetheless, 4/6 contained significant steatosis (Table 1) and 2/6 showed a hypovascular pattern (Fig. 4) that led to misclassification in H-HCA subtype in MRI.

UHCA MRI features ($n = 9$)

No specific MRI characteristics were found in UHCA. Most UHCAs presented necrotic/hemorrhagic remodeling > 50% (7/9) and no fatty component was observed in this subtype. All of them were positive to Ass1 in immunohistochemistry.

Multiple HCAs

Multiple HCA (≥ 10 nodules, i.e., adenomatosis) were found in 14 cases of H-HCA and 13 cases of IHCA on pathologic examination, whereas only 11 H-HCA and 9 IHCA cases of those multiple HCAs were visible on MRI, because some micro-adenomas (< 5 mm) observed on pathologic examination were not identified by MRI.

3/86 patients (3%) presented both H-HCA and IHCA subtypes and 4/86 (5%) patients both IHCAs and b-IHCAs.

Complications

Hemorrhage

All subtypes were affected by hemorrhagic changes (24/116, 21%), especially UHCA (7/9, 78%) and b-HCA (2/6, 33%), though in small number. No significant bleeding rate difference was found between the two major subtypes: 6/43 H-HCAs (14%) vs. 9/58 IHCAs (15%), $p = 0.827$. The median size of hemorrhagic HCAs was 6.5 cm vs. 4.5 cm for non-hemorrhagic HCAs ($p < 0.001$). No significant size difference was found between phenotypes among hemorrhagic HCAs ($p = 0.243$). Severity of bleeding was low in the majority, with 20/24 (83%) grade I bleeds, 4/24 (17%) grade II and no grade III listed. No hemorrhagic change was found below 4.2 cm regardless of phenotype and a cutoff to ≤ 5 cm was associated with a negative predictive value for bleeding of 94.8%(3 grade I bleeds ≤ 5 cm).

Malignant transformation

Cases of malignant transformation were more frequent in males (3/12 nodules) than in females (3/104 nodules), $p = 0.014$. b-HCAs and b-IHCA represented 67% of cases (4/6), but other subtypes may be concerned (Table 1). Four MRI "nodule-in-nodule" features (Fig. 5) were identified and correlated to 4 well-differentiated HCC/dysplastic/or borderline area cases identified by pathologists. MRI could not identify 2 other cases of borderline HCAs: one with microscopic borderline foci and another case with severe necrotic/hemorrhagic changes leading to interpretation difficulties. Borderline HCAs were characterized by cytological atypia and/or architectural atypia, but these features were not sufficient for diagnosis of HCC. Regardless of subtype, no malignant transformation was seen below a tumor size of < 5.2 cm.

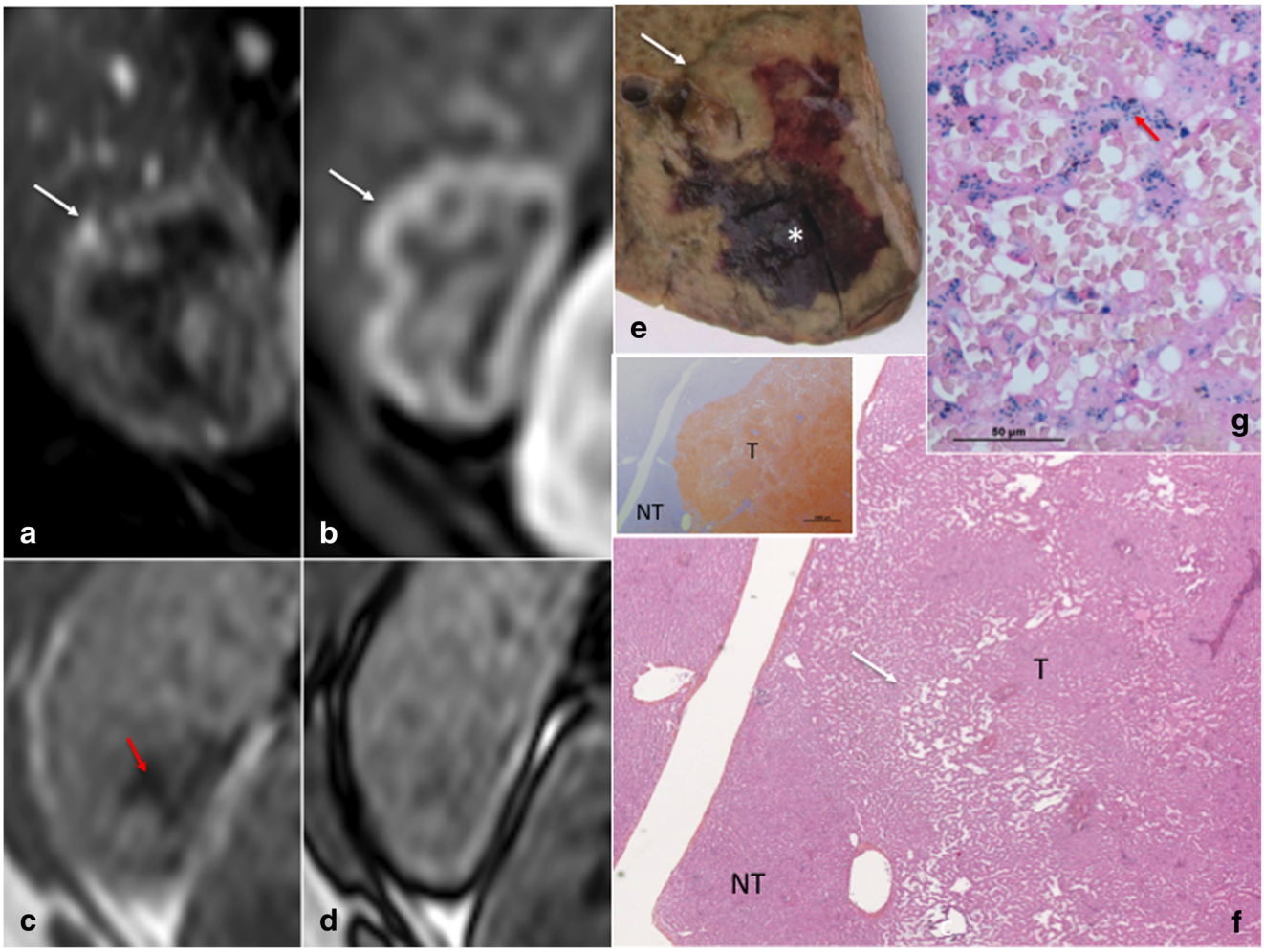

Fig. 3 Inflammatory HCA (IHCA) with central hemosiderin deposits. **a**, **b**, **c**, **d** Axial T2-weighted (**a**), three-dimensional fat-suppressed gradient-echo T1-weighted after injection of gadolinium chelate at the arterial phase (**b**), in phase (**c**), and opposed phase (**d**) T1-weighted gradient-echo sequence. Tumor (3.2 cm; segment VI) with peripheral signs of hyperintense sinusoidal dilatation (crescent sign, white arrows) on T2W (**a**) with arterial enhancement (**b**) and a remodeled central area with hypointense iron deposits both on T2W (**a**) and in phase (**c**) gradient echo sequence (magnetic susceptibility artifact, red arrow); **e** formalin fixed specimen. Tumor with a large congestive area (*); **f** *H&E*, tumor (T) made of benign hepatocytes with obvious sinusoidal dilatation predominantly at the periphery (white arrow); *inset, upper left*: *CRP immunostaining*, diffuse overexpression of CRP in T, well demarcated from the non-tumoral liver (NT).**g** *Perls staining*, hemosiderin (red arrow) stained in blue in hepatocytes, red blood cells in dilated sinusoids

Discussion

New MRI features

In the largest series to date, we identified two main MRI features associated with the two major HCA subtypes: (a) hypovascular pattern associated with a fat component (homogeneous or heterogeneous) for H-HCA; (b) and crescent sign (partial rim of SD whatever the appearance of the center of the lesion) for IHCA, and proposed new highly sensitive and specific MRI criteria that improve the performance of MRI diagnosis.

Considering H-HCAs, they were mainly characterized by fatty phenotype [16, 18, 25]. Among all H-HCA, 67% were identified by classical criteria [16]. Unlike previous reports [16–18], 33% with moderate to low and heterogeneous steatosis remained non-diagnosed using classical criteria with a sensitivity of 67.4% vs. 86.7% [16] and 90.9% [17], respectively, in previously smaller series. We found that our new criteria, i.e., association of fatty component and hypovascular pattern allowed for the correct reclassification of 21% of H-HCAs.

Considering IHCAs, they were mainly characterized by sinusoidal dilatation (88%). Classical MRI criteria [16, 18] were present in 37/58 (64%) cases. However, the presence of fatty and/or necrotic/hemorrhagic components led to failed IHCA characterization using these criteria [16, 18] with an observed sensitivity of 63.8% in this cohort vs. 85.2% [16] and 82.4% [17] in previous, smaller series. Our isolated peripheral "crescent" of sinusoidal dilatation significantly improved the characterization of

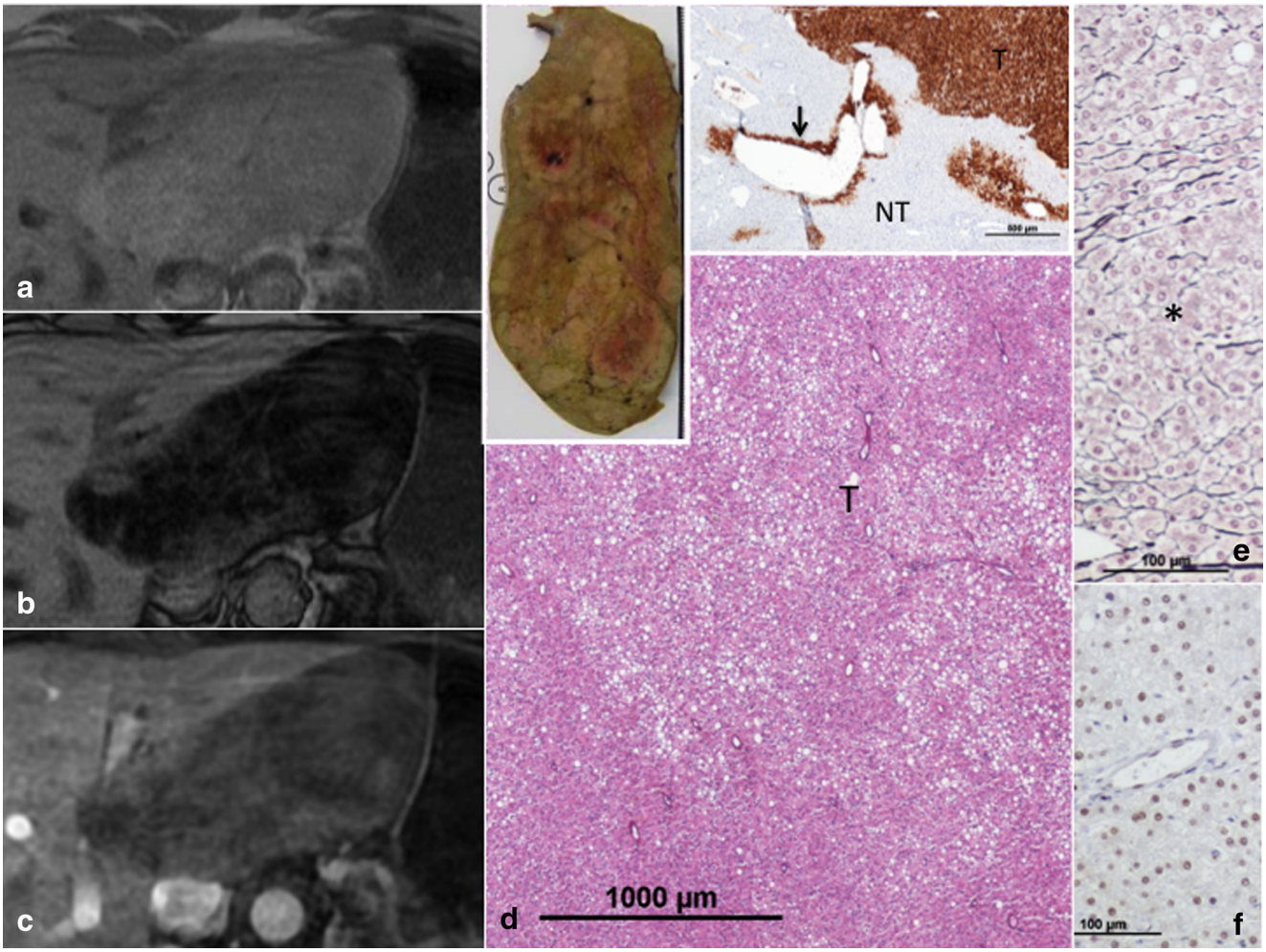

Fig. 4 Steatotic β-catenin-activated HCA (b-HCA) with "borderline" foci and hypovascular pattern on MRI. **a**, **b**, **c** Axial in phase (**a**) and opposed phase (**b**) T1-weighted gradient-echo sequence, axial fat suppressed gradient-echo T1-weighted after injection of gadolinium chelate at portal venous phase (**c**). Large steatotic tumor (12 cm; segments II-III) with strong but heterogeneous signal dropout on out-phase (**b**) and hypovascular pattern (**c**); **d** *H&E*, well-differentiated hepatocellular tumor (T), irregularly disseminated steatosis, intermingled with numerous thin arterioles; *inset upper left*: *formalin-fixed specimen*, multinodular brown/yellowish tumor; *inset upper right*: *glutamine synthetase (GS) immunostaining*, strong and diffuse expression of GS in T, whereas GS is normally expressed in a few rows of perivenular hepatocytes (arrow) in non-tumoral liver (NT); **e** *reticulin staining*, decreased and irregular reticulin network in some areas of the tumor (*); **f** *Heat Shock protein (HSP)*, numerous nuclei expressed HSP in some tumoral foci

IHCAs, reaching a sensitivity of 87.9% and a specificity of 100%, whatever the tissue changes (necrotic, hemorrhagic, fatty changes) in the center of the lesion. Moreover, central hemosiderin deposits are very useful specific signs of IHCAs in association with sinusoidal dilatation.

Failure to classify with MRI

Despite the high accuracy of the proposed new criteria (only 11.6% of H-HCAs and 12% of IHCAs remaining non-diagnosed), MRI failed to classify subtypes in five situations: (*1*) area of necrotic/hemorrhagic remodeling exceeding 50% of tumor area in H-HCAs and IHCAs subtypes; (*2*) H-HCAs without any fatty component, (*3*) IHCAs without sinusoidal dilatation confirmed by microscopic examination (*4*) b-HCAs, and (*5*) UHCAs.

Considering H-HCAs and IHCAs, 80% of non-diagnosed H-HCAs (4/5) and 43% of non-diagnosed IHCAs (3/7), based on the new criteria, were remodeled by over 50%.

Considering b-HCAs, no specific characteristic able to differentiate β-catenin-mutated from other subtypes was found. No genuine specific central scar [18] and no delayed wash-out [16] were observed. We still showed that b-HCAs could display a misleading steatotic appearance [26] with hypovascular pattern. However, it is difficult to draw robust conclusions because b-HCAs represent a small number of cases.

Furthermore, MRI was not able to distinguish b-IHCAs from IHCAs.

Unfortunately, to date, only pathologic data are able to diagnose β-catenin-activated HCAs. Preliminary data suggest that hepatobiliary-specific contrast agents [27, 28] could

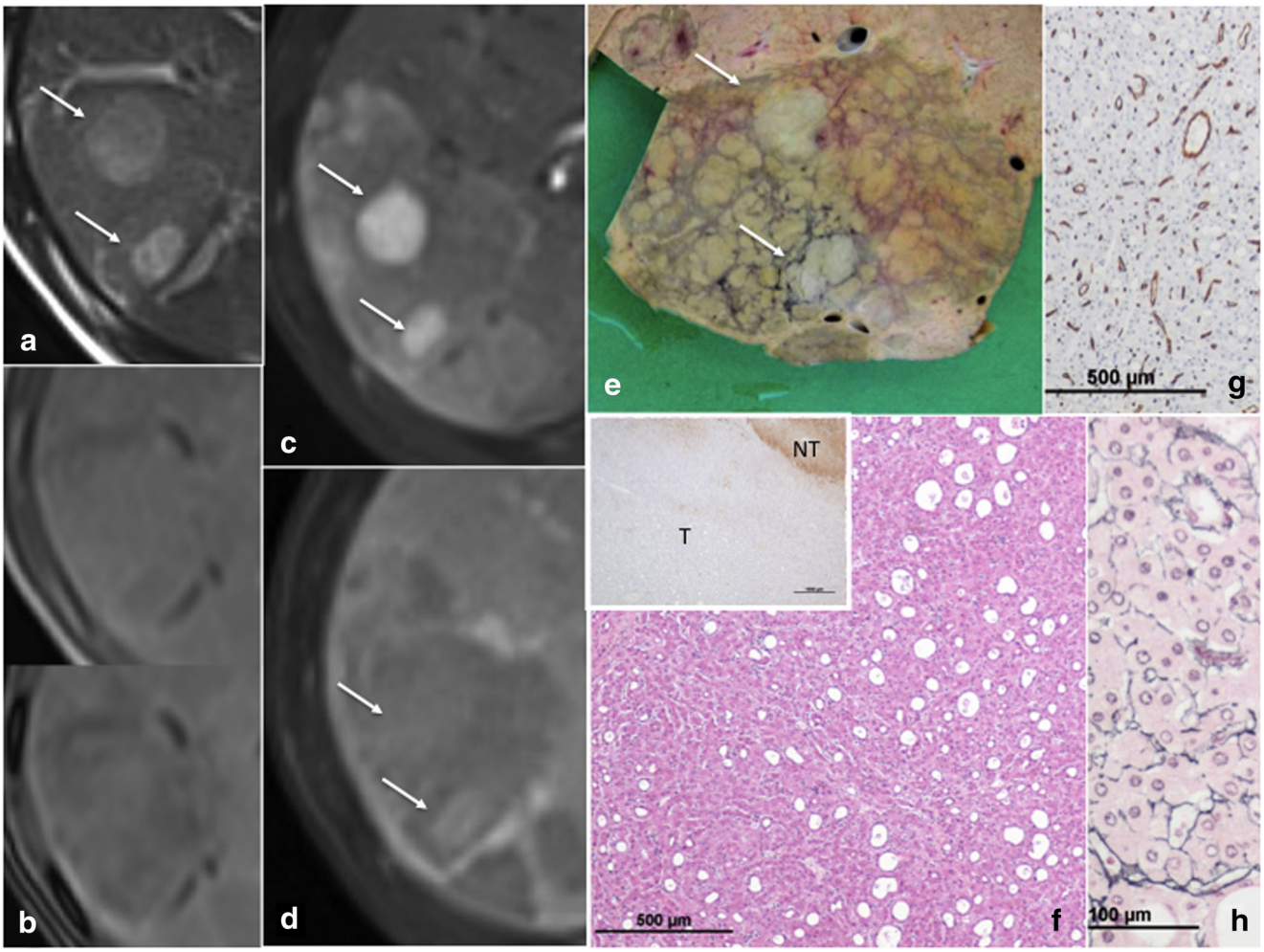

Fig. 5 HNF1a-inactivated (H-HCA) adenomatosis with foci of malignant transformation (borderline/HCC). **a**, **b**, **c**, **d** Axial FS T2W (**a**), in phase and opposed phase T1W GRE (**b**), axial T1W fat-suppressed gradient-echo after gadolinium administration at arterial (**c**) and portal venous phases (**d**). Lesion (8.5 cm; segments VII-VIII) showing two MRI "nodule-in-nodule" features (white arrows), hyperintense on T2W (**a**), with strong arterial enhancement (**c**) and persistent portal venous enhancement (**d**) (the upper nodule displaying near wash-out); weak signal dropout on out-phase (**b**) (low fatty component); **e** *formalin-fixed specimen*, polychrome multinodular tumor with two whitish nodules (white arrows); **f** *H&E*, well-differentiated hepatocellular tumor, with numerous glandular structures; *inset upper left*: lack of LFABP expression in the tumor (T), contrasting with normal expression in adjacent non-tumoral liver (NT); **g** *CD34 immunostaining*, numerous arteries, and diffuse sinusoidal capillarization; **h** *reticulin staining*, decreased and irregular reticulin network

provide additional valuable information because some b-HCA can appear iso- to hyperintense in hepatobiliary phase. However, these cases represent a minority of b-HCA [29], and I-HCA can also present enhancement at HBP [28, 29].

Considering UHCAs, the importance of remodeling following necrotic/hemorrhagic changes leads to both pathology and MRI analysis-related difficulties [15].

Bleeding and malignant transformation risks

Despite a reputed increased bleeding risk in IHCAs [30, 31], no significant difference was found in our series between H-HCA and IHCA, as seen [10, 32]. Although hemorrhagic changes can lead to size misestimation [32], the risk of bleeding and rupture of small lesions seemed to be minimal (none below 4.2 cm).

In addition to what is commonly described in b-HCAs [10, 34–36], we observed malignancy in H-HCA subtype, in a male with liver vascular disorder related to Fallot tetralogy [11, 33, 34]. MRI allowed to detect macroscopic areas of well-differentiated HCC transformation with the "nodule-in-nodule" feature, but borderline foci lesions could be missed.

Limits and perspectives

Our retrospective study had several exclusions because of lack of suitable MRI data, but we consider our large series sufficient to make strong observations especially for rare

tumors. Diffusion sequences were not included in the analysis, but even if diffusion could be helpful for distinguish FNH from HCA [35, 36], no study had shown until now its interest to distinguish HCA subtypes, with no significant difference for ADC values between each subtype [36]. Hepatobiliary phase was not included in MRI criteria, but if HBP had an interest to distinguish FNH from HCA with usually FNH in iso- or hyperintensity and HCA in hyposignal in HBP [29, 37], caution must be taken because some HCA especially b-HCA and IHCA can appear iso- to hyperintensity in HBP related to over expression of OATP1B1/3 and/or decrease or no expression of MRP3 leading to contrast-media retention and could create a diagnostic dilemma [28, 29].

Conclusion

We identified several non-described MRI features that improve the classification of the two major HCA subtypes. In addition to the classical criteria, these new criteria contribute to the identification of 88% of the two major HCA subtypes in discriminating low to moderate steatotic H-HCAs with "hypovascular pattern," and remodeled IHCAs bearing a peripheral "crescent sign" of sinusoidal dilatation. Malignant transformation occurred in 5% of cases, and bleeding in 20% with low severity in 83%.

Acknowledgments We thank Professors Jean Saric and Laurence Chiche (surgeons); Brigitte Le Bail and Dr. Claire Castain (liver pathologists); and Florent Maire for their clinical contributions to this study.

Funding The authors state that this work has not received any funding.

Compliance with ethical standards

Guarantor The scientific guarantor of this publication is Dr. Frulio Nora.

Conflict of interest The authors of this manuscript declare no relationships with any companies, whose products or services may be related to the subject matter of the article.

Statistics and biometry No complex statistical methods were necessary for this paper.

Informed consent Written informed consent was waived by the Institutional Review Board.

Ethical approval Institutional Review Board approval was obtained.

Study subjects or cohorts overlap Some study subjects (30 cases) have been previously reported in Hepatology 2008 by Laumonier et al—Hepatocellular adenomas: magnetic resonance imaging features as a function of molecular pathological classification.

Methodology
- Retrospective
- Diagnostic or prognostic study
- Performed at one institution

References

1. Rooks JB, Ory HW, Ishak KG et al (1979) Epidemiology of hepatocellular adenoma. The role of oral contraceptive use. JAMA 242: 644–648
2. Nault JC, Bioulac-Sage P, Zucman-Rossi J (2013) Hepatocellular benign tumors-from molecular classification to personalized clinical care. Gastroenterology 144:888–902
3. Bioulac-Sage P, Rebouissou S, Thomas C et al (2007) Hepatocellular adenoma subtype classification using molecular markers and immunohistochemistry. Hepatology 46:740–748
4. Bioulac-Sage P, Balabaud C, Zucman-Rossi J (2010) Subtype classification of hepatocellular adenoma. Dig Surg 27:39–45
5. Paradis V, Benzekri A, Dargère D et al (2004) Telangiectatic focal nodular hyperplasia: a variant of hepatocellular adenoma. Gastroenterology 126:1323–1329
6. Bioulac-Sage P, Rebouissou S, Sa Cunha A et al (2005) Clinical, morphologic, and molecular features defining so-called telangiectatic focal nodular hyperplasias of the liver. Gastroenterology 128: 1211–1218
7. Rebouissou S, Amessou M, Couchy G et al (2009) Frequent in-frame somatic deletions activate gp130 in inflammatory hepatocellular tumours. Nature 457:200–204
8. Pilati C, Amessou M, Bihl MP et al (2011) Somatic mutations activating STAT3 in human inflammatory hepatocellular adenomas. J Exp Med 208:1359–1366
9. Nault JC, Fabre M, Couchy G et al (2012) GNAS-activating mutations define a rare subgroup of inflammatory liver tumors characterized by STAT3 activation. J Hepatol 56:184–191
10. Bioulac-Sage P, Laumonier H, Couchy G et al (2009) Hepatocellular adenoma management and phenotypic classification: the Bordeaux experience. Hepatology 50:481–489
11. Zucman-Rossi J, Jeannot E, Nhieu JT et al (2006) Genotype-phenotype correlation in hepatocellular adenoma: new classification and relationship with HCC. Hepatology 43:515–524
12. Stoot JH, Coelen RJ, De Jong MC, Dejong CH (2010) Malignant transformation of hepatocellular adenomas into hepatocellular carcinomas: a systematic review including more than 1600 adenoma cases. HPB (Oxford) 12:509–522
13. Van der Borght S, Libbrecht L, Katoonizadeh A et al (2007) Nuclear beta-catenin staining and absence of steatosis are indicators of hepatocellular adenomas with an increased risk of malignancy. Histopathology 51:855–856
14. Nault JC, Couchy G, Balabaud C et al (2017) Molecular classification of hepatocellular adenoma associates with risk factors, bleeding, and malignant transformation. Gastroenterology 152:880–894 e6
15. Henriet E, Abou Hammoud A, Dupuy JW et al (2017) Argininosuccinate synthase 1 (ASS1): a marker of unclassified hepatocellular adenoma and high bleeding risk. Hepatology 66: 2016–2028
16. Laumonier H, Bioulac-Sage P, Laurent C, Zucman-Rossi J, Balabaud C, Trillaud H (2008) Hepatocellular adenomas: magnetic resonance imaging features as a function of molecular pathological classification. Hepatology 48:808–818
17. Ronot M, Bahrami S, Calderaro J et al (2011) Hepatocellular adenomas: accuracy of magnetic resonance imaging and liver biopsy in subtype classification. Hepatology 53:1182–1191

18. van Aalten SM, Thomeer MG, Terkivatan T et al (2011) Hepatocellular adenomas: correlation of MR imaging findings with pathologic subtype classification. Radiology 261:172–181
19. Grazioli L, Olivetti L, Mazza G, Bondioni MP (2013) MR imaging of hepatocellular adenomas and differential diagnosis dilemma. Int J Hepatol 2013:374170
20. Wu JS, Hochman MG (2009) Soft-tissue tumors and tumorlike lesions: a systematic imaging approach. Radiology 253:297–316
21. Salaria SN, Graham RP, Aishima S, Mounajjed T, Yeh MM, Torbenson MS (2015) Primary hepatic tumors with myxoid change: morphologically unique hepatic adenomas and hepatocellular carcinomas. Am J Surg Pathol 39:318–324
22. Merkle EM, Nelson RC (2006) Dual gradient-echo in-phase and opposed-phase hepatic MR imaging: a useful tool for evaluating more than fatty infiltration or fatty sparing. Radiographics 26: 1409–1418
23. Bieze M, Phoa SS, Verheij J, van Lienden KP, van Gulik TM (2014) Risk factors for bleeding in hepatocellular adenoma. Br J Surg 101: 847–855
24. DeLong ER, DeLong DM, Clarke-Pearson DL (1988) Comparing the areas under two or more correlated receiver operating characteristic curves: a nonparametric approach. Biometrics 44:837–845
25. Tse JR, Naini BV, Lu DS, Raman SS (2016) Qualitative and quantitative gadoxetic acid-enhanced MR imaging helps subtype hepatocellular adenomas. Radiology 279:118–127
26. Ishii M, Kazaoka J, Fukushima J et al (2015) A case of beta-catenin-positive hepatocellular adenoma with MR imaging sign of diffuse intratumoral fat deposition. Abdom Imaging 40:1487–1491
27. Yoneda N, Matsui O, Kitao A et al (2012) Beta-catenin-activated hepatocellular adenoma showing hyperintensity on hepatobiliary-phase gadoxetic-enhanced magnetic resonance imaging and overexpression of OATP8. Jpn J Radiol 30:777–782
28. Ba-Ssalamah A, Antunes C, Feier D et al (2015) Morphologic and molecular features of hepatocellular adenoma with gadoxetic acid-enhanced MR imaging. Radiology 277:104–113
29. Guo Y, Li W, Cai W, Zhang Y, Fang Y, Hong G (2017) Diagnostic value of gadoxetic acid-enhanced MR imaging to distinguish HCA and its subtype from FNH: a systematic review. Int J Med Sci 14: 668–674
30. Belghiti J, Cauchy F, Paradis V, Vilgrain V (2014) Diagnosis and management of solid benign liver lesions. Nat Rev Gastroenterol Hepatol 11:737–749
31. Dokmak S, Paradis V, Vilgrain V et al (2009) A single-center surgical experience of 122 patients with single and multiple hepatocellular adenomas. Gastroenterology 137:1698–1705
32. van Aalten SM, de Man RA, IJzermans JN, Terkivatan T (2012) Systematic review of haemorrhage and rupture of hepatocellular adenomas. Br J Surg 99:911–916
33. Bioulac-Sage P, Sempoux C, Possenti L et al (2013) Pathological diagnosis of hepatocellular cellular adenoma according to the clinical context. Int J Hepatol 2013:253261
34. Sempoux C, Paradis V, Komuta M et al (2015) Hepatocellular nodules expressing markers of hepatocellular adenomas in Budd-Chiari syndrome and other rare hepatic vascular disorders. J Hepatol 63: 1173–1180
35. Agnello F, Ronot M, Valla DC, Sinkus R, Van Beers BE, Vilgrain V (2012) High-b-value diffusion-weighted MR imaging of benign hepatocellular lesions: quantitative and qualitative analysis. Radiology 262:511–519
36. Zarghampour M, Fouladi DF, Pandey A et al (2018) Utility of volumetric contrast-enhanced and diffusion-weighted MRI in differentiating between common primary hypervascular liver tumors. J Magn Reson Imaging. https://doi.org/10.1002/jmri.26032
37. Reizine E, Amaddeo G, Pigneur F et al (2018) Quantitative correlation between uptake of Gd-BOPTA on hepatobiliary phase and tumor molecular features in patients with benign hepatocellular lesions. Eur Radiol. https://doi.org/10.1007/s00330-018-5438-7